

1
2
3 **A “frozen volume” transition model and working mechanism for the shape**
4
5 **memory effect in amorphous polymers**
6

7 Haibao Lu^{1,3}, Xiaodong Wang¹, Yongtao Yao¹ and Yong Qing Fu²
8
9

10 ¹National Key Laboratory of Science and Technology on Advanced Composites in Special
11 Environments Laboratory, Harbin Institute of Technology, Harbin 150080, China
12
13

14 ²Faculty of Engineering and Environment, Northumbria University, Newcastle upon Tyne,
15 NE1 8ST, UK
16
17

18 ³E-mail: luhb@hit.edu.cn (H. Lu)
19
20
21

22 **Abstract:** Phenomenological models based on frozen volume parameters could well predict
23 shape recovery behavior of shape memory polymers (SMPs), but the physical meaning of
24 using the frozen volume parameters to describe thermomechanical properties has not been
25 well-established. In this study, the fundamental working mechanisms of the shape memory
26 effect (SME) in amorphous SMPs, whose temperature-dependent viscoelastic behavior
27 follows the Eyring equation, have been established with the considerations of both internal
28 stress and its resulted frozen volume. The stress-strain constitutive relation was initially
29 modeled to quantitatively describe effects of internal stresses at the macromolecular scale
30 based on the transient network theory. A phenomenological “frozen volume” model was then
31 established to characterize the macromolecule structure and SME of amorphous SMPs based
32 on a two-site stress-relaxation model. Effects of the internal stress, frozen volume and strain
33 rate on shape memory behavior and thermomechanical properties of the SMP were
34 investigated. Finally, the simulation results were compared with the experimental results
35 reported in the literature, and good agreements between the theoretical and experimental
36 results were achieved. The novelty and key differences of our newly proposed model with
37
38
39
40
41
42
43
44
45
46
47
48
49
50
51
52
53
54
55
56
57
58
59
60

1
2
3
4 respect to the previous reports are (1). The “frozen volume” in our study is caused by the
5
6 internal stress and governed by the two-site model theory, thus has a good physical meaning.
7
8
9 (2). The model can be applied to characterize and predict both the thermal and
10
11 thermomechanical behaviors of SMPs based on the constitutive relationship with internal
12
13 stress parameters. It is expected to provide a power tool to investigate the thermomechanical
14
15 behavior of the SMPs, of which both the macromolecular structure characteristics and SME
16
17 could be predicted using this “frozen volume” model.
18
19
20
21

22 **Keywords:** Shape memory polymer; amorphous polymer; phenomenological model
23
24
25
26

27 **1. Introduction**

28
29
30 Shape memory polymer (SMP) is one type of smart materials that could respond to the
31
32 environmental stimuli and then change their shapes according to the predetermined functions
33
34 and programmed designs [1]. It is featured by the capability of regaining its permanent shape
35
36 (after being pre-deformed) after proper stimuli, including temperature, water, solvent, light,
37
38 electric or magnetic fields [2-4]. In contrary to the shape memory alloys or shape memory
39
40 ceramics, SMPs have the advantage being lightweight, low cost and potential good
41
42 biocompatibility, but produce relatively lower recovery stresses during deformation [5-7].
43
44 Therefore, they have been extensively researched, both experimentally and theoretically, to
45
46 explore their various potential applications. As it is well-known, modelling based on
47
48 thermo-viscoelasticity is commonly used to characterize and predict the shape memory
49
50 behavior of the SMPs [8-11]. Previously published papers reported that the stresses applied to
51
52 the elastic springs (i.e., the hard segment) provided the driving force for free recovery of the
53
54
55
56
57
58
59
60

1
2
3
4 SMPs [12-14], which caused a decrease in potential barrier thus the activation of frozen
5
6 molecules [15]. These results showed that it is important to investigate the effects of driving
7
8 force and activation energy on the SME of the SMPs. The shape memory behavior of the
9
10 SMPs generally follows the Eyring equation and Williams-Landel-Ferry (WLF) equation, as
11
12 widely reported in literature [16-18].
13
14

15
16
17 In terms of thermodynamics, SMPs can be treated as a mixture of active and frozen phases,
18
19 where the frozen phases will change into active phases after the SMPs are heated above their
20
21 glass transition temperatures [19,20]. For example, Liu et al proposed a theoretical model for
22
23 amorphous SMPs which incorporated the active and frozen phases in the macromolecules
24
25 [12]. Long et al further developed a dynamic model for the phase transition of the frozen
26
27 phases during which the SMP undergoes the glass transition [9]. However, in the above
28
29 studies, only the temperature effect on the transition of frozen phases has been considered,
30
31 and the effects of time or stress have not been investigated. Therefore, Xiao and Guo
32
33 proposed a constitutive relation considering the relaxation time and applied stress as a
34
35 function of the frozen fraction in SMPs [21,22]. These theoretical studies have demonstrated
36
37 their capabilities to describe the thermomechanical performance and SME of the SMPs.
38
39 However, it should be pointed that the frozen volume parameter does not have clear physical
40
41 meanings, and the internal stress in the SMP has not been considered in those models.
42
43 Therefore, a phenomenological model is critically needed to predict and describe both the
44
45 internal stress and frozen volumes and their transition behaviors. By means of combining the
46
47 influences of temperature and strain rate, the internal stress and the resulted “frozen volume”
48
49 are correlated with the shape/temperature memory behavior across the glass transition
50
51
52
53
54
55
56
57
58
59
60

temperature of the SMPs based on the Eyring model [23]. The energy stored in the SMP is formulated based on the “frozen volume” method. In the subsequent recovery process, the release rate of strain energy is consistent with the activation rate of “frozen volume”.

In this study, a two-site model [17] was initially introduced to construct a constitutive relation between activation energy (which turns the frozen phase into the active phase) with applied stress (σ_a) and internal stress (σ_i), where the quantity of $(-d \ln \left(\frac{\dot{\sigma}_a}{\sigma_a} \right)) / d\sigma_a$ was presented as the experimental fraction of the frozen volume. The constitutive equations for the internal stress, strain rate and glassy transition temperatures were further constructed by means of the transient network theory. Finally, the simulation results were compared with those experimental ones reported in the literature for validations.

2. Influence of internal stress on SME in a free recovery process of SMP

Generally a fully melting happens at a temperature which is a few degrees above T_g . This temperature is named as T_h . Based on the previous work [24-26], the temperature dependence on the internal stress $\sigma_i(t)$ has the following expression,

$$\sigma_i(T) = \sigma_i(0) - \frac{T}{T_{ref}} (\sigma_i(0) - \sigma_i(T_{ref})) \quad \sigma_i(T_{ref}) = 0 \quad (1)$$

where $\sigma_i(0)$ is the internal stress at 0 K, T and T_{ref} represent the temperature and reference temperature, respectively. When the reference temperature is T_h , a linear relationship between the internal stress and temperature can be found and is written as,

$$\sigma_i(T) = \sigma_i(0) - \frac{T}{T_h} (\sigma_i(0) - \sigma_i(T_h)) \quad \sigma_i(T_h) = 0 \quad (2)$$

According to the thermodynamics of polymer, the existence of the stress will reduce the barrier height of the soft segments in the SMPs [27]. The volume of these soft segments is

1
2
3
4 defined as the “frozen volume”, which will be activated in accompany with state/phase
5
6 transitions caused by the driving force in the process of shape recovery; and the change in
7
8 barrier height is the product of both the driving force and frozen volume. Figure 1 shows the
9
10 reduced energy barrier produced by the driving force, in which ΔG denotes the potential
11
12 barrier without the influence of the stress, and v denotes the frozen volume caused by the
13
14 driving force (σ).
15
16
17
18

19 Here γ is used to express the probability of a molecule to be **activated** at a certain
20
21 temperature. An Eyring form is proposed to describe this probability as follows,
22
23

$$\gamma = AT \exp\left(-\frac{\Delta G(T)-v\sigma}{k_B T}\right) \quad (3)$$

24
25
26
27
28 where $\Delta G(T)$ is the energy barrier without applying driving force and it changes with
29
30 temperature; k_B is the Boltzmann constant, T is the absolute temperature, v is the frozen
31
32 volume caused by the applied stress, σ is the driving force, and A represents the correction
33
34 constant.
35
36
37
38

39 Firstly the condition of the free recovery process of the SMP is considered, i.e., only the
40
41 temperature has been changed while the applied stress is zero. In this case, the internal stress
42
43 will be acted as the driving force, instead of the applied stress. It was reported that the applied
44
45 stress has a linear relationship with the internal stress [23], thus the frozen volume, v , caused
46
47 by the internal stress will follow the form $(d \ln(-\dot{\sigma}_a))/d\sigma_a$ and can be written **as**
48
49

$$v = \left(d \ln \left(-\dot{\sigma}_a \right) \right) / d\sigma_i.$$

50
51
52
53
54 Assuming that there is no influence of the population distribution of the different types of
55
56 sites available to the elements, the frozen volume caused by the internal stress σ_i can be
57
58
59
60

expressed as follows based on the two-site model theory [17]:

$$v = d \ln \left(-\dot{\sigma}_a \right) / d\sigma_i = k_B T \frac{C}{C\sigma_i(T) - D\sigma_i(0)} \quad (4)$$

where C and D are the constants in the investigated temperature range. To simplify equation (4), we define two constants a and b as follows,

$$\frac{1}{\sigma_i(0)} = a \quad 1 - \frac{D}{C} = b \quad (5)$$

Thus,

$$v = \frac{a}{b - \frac{T}{T_h}} k_B T \quad (6)$$

By combining equations (2) and (6), we can obtain,

$$v\sigma = \left[\sigma_i(0) - \frac{T}{T_h} (\sigma_i(0) - \sigma_i(T_h)) \right] \left(\frac{a}{b - \frac{T}{T_h}} \right) k_B T \quad (7)$$

Because $\sigma_i(T_h)=0$ and $\frac{1}{\sigma_i(0)} = a$, by substituting equation (7) into (3), a full expression

form of γ can be obtained,

$$\gamma = AT \exp \left(\frac{-\Delta G(T) + \left(\frac{T_h - T}{b \cdot T_h - T} \right) k_B T}{k_B T} \right) \quad (8)$$

Here it is considered that the unit of ΔG is J/mol . Equation (10) can be rewritten by multiplying N_A on the numerator and denominator,

$$\gamma = AT \exp \left(\frac{-\Delta G(T) + \left(\frac{T_h - T}{b \cdot T_h - T} \right) RT}{RT} \right) \quad (R = k_B N_A) \quad (9)$$

where R is the universal gas constant and N_A is the **Avogadro's** number.

As temperature increases, the internal energy of the SMPs will be increased accordingly,

thus causing the decreases of potential barrier of the soft segments. WLF equation was used here to express the changes in mobility of the molecules in frozen phase. If the mobility is increased, less energy is needed in the activation process. The Gibbs activation energy ΔG as a function of temperature can be described using the following equation [18],

$$\Delta G(T) = \Delta G(T_h) 10^{\frac{-C_1(T-T_h)}{C_2+T-T_h}} \quad (10)$$

where $\Delta G(T_h)$ represents the activation energy at a temperature of T_h . C_1 and C_2 are constants.

By substituting equation (10) into (9), we can obtain the final formulation of γ ,

$$\gamma = AT \exp\left(-\frac{\Delta G(T_h) 10^{\frac{-C_1(T-T_h)}{C_2+T-T_h}}}{RT} + \frac{T_h - T}{b \cdot T_h - T}\right) \quad (11)$$

The decrease of activation energy ΔG (which turns the frozen phase into the active one of the macromolecules) caused by the existence of internal stresses is set as $\Delta G(\sigma_i)$. For a unit volume of pre-deformed amorphous SMP, the frozen fraction ϕ_f which is linked with the frozen volume has the following form,

$$\phi_f = 1 - \gamma = 1 - AT \exp\left(-\frac{\Delta G(T_h) 10^{\frac{-C_1(T-T_h)}{C_2+T-T_h}}}{RT} + \frac{T_h - T}{b \cdot T_h - T}\right) \quad (12)$$

In order to verify the accuracy of equation (12), a comparison between the simulation result of the model with the reported experimental one is prepared [12]. According to the robust global optimization (RGO) method, the parameters of $A = 0.00337$, $C_1 = 9.65$, $C_2 = 200\text{K}$, $\Delta G(T_h) = 578.5\text{J/mol}$ and $b = 1.07$ have been used. Figure 2 plots the numerical results for the frozen volume fraction as a function of the temperature (T/T_g), and the experimental data are also plotted for comparisons. Simulation results reveal that the frozen

1
2
3
4 volume fraction of the SMPs decreases nonlinearly and the rate of the decrease becomes
5
6 **significantly** with an increase in temperature. At 358K, the phase transition finishes, and the
7
8 frozen volume fraction **turns into** zero. Furthermore, it is found that the theoretical simulation
9
10 results are in good **agreements** with the experimental results. The simulation results
11
12 theoretically confirm that the phenomenological frozen volume fraction has a **good physical**
13
14 meaning to account for the phase/state transitions in the shape recovery process of SMPs. The
15
16 relationship between the frozen volume fraction and temperature provides an effective
17
18 approach to depict and predict the SME in SMPs. In comparison with the polynomial
19
20 **expressions** for the frozen fraction proposed by Liu et al [12], **our newly proposed** model (i.e.,
21
22 equation 12) has the advantages to provide a physical and mathematic relationship between
23
24 the energy barrier ΔG parameter and the frozen volume, which is originated from the
25
26 internal stress.
27
28
29
30
31
32
33
34

35 According to equation (10), the decreases of the activation energy caused by the increases
36
37 of internal stress and temperature are shown in **Figure 3(a)**. It is found that both the values of
38
39 $\Delta G(\sigma_i)$ and $\Delta G(T)$ have a nonlinear relationship with the temperature. With the increase
40
41 of temperature, the quantity of $\Delta G(\sigma_i)$ decreases sharply whereas that of $\Delta G(T)$
42
43 decreases slowly. From equations (2) and (4), the frozen volume caused by the internal stress
44
45 increases with the increase of temperature, and the driving force **has** a linear relationship with
46
47 temperature. Therefore, at a higher temperature, the increase rate of frozen volume caused by
48
49 the increased driving force becomes smaller. When the temperature reaches T_h , not only the
50
51 phase transition ends, but also the frozen volume induced by the driving force turns to zero. It
52
53 is considered that the driving force is zero when the phase transition finishes, therefore,
54
55
56
57
58
59
60

1
2
3
4 without the driving force, the frozen volume caused by the driving force will disappear. As
5
6 presented in Figure 3(b), as the temperature is increased to the glass transition temperature
7
8 (i.e., 343K), the effect of driving force on the activation energy become significant.

9
10
11 Effect of the parameter b on the $\Delta G(\sigma_i)$ has been further studied and the simulation
12
13 results are plotted in Figure 4(a). It is revealed that the curves of the $\Delta G(\sigma_i)$ are decreased
14
15 with the increase in the activation volume at different values of $b=1.05, 1.07, 1.09, 1.11$ and
16
17 1.13. While b is set as 2, 3, 4, 5 and 6, the simulation results of $\Delta G(\sigma_i)$ are plotted in
18
19 Figure 4(b). It is found that $\Delta G(\sigma_i)$ decreases proportionally with the parameter b at a
20
21 given temperature. With an increase in the value of the parameter b , the slopes of curves
22
23 become decreased.
24
25
26
27
28
29

30 Furthermore, the decrease of activation energy is also determined by the driving force and
31
32 temperature based on equation (11) as shown in Figure 5(a). Below the temperature of 333 K
33
34 (the glass transition temperature is 343 K), values of $\Delta G(\sigma_i)$ are less than ten percent of
35
36 those of $\Delta G(T)$, and the contribution of the decrease of activation energy caused by the
37
38 driving force can be negligible. Therefore, the influence of $\Delta G(\sigma_i)$ could be neglected at a
39
40 low temperature range. However, when the temperature is above 333 K, the influence of
41
42 $\Delta G(\sigma_i)$ becomes significant and has a strong influence on the decrease of the activation
43
44 energy. The peak value of the specific value of $\Delta G(\sigma_i)/\Delta G(T)$ was obtained at a
45
46 temperature of 351.5 K and the value is 0.493. This value decreases significantly when the
47
48 temperature is over 351.5 K. As the parameter b is increased from 1.03, 1.04, 1.05 to 1.06, the
49
50 numerical results of $\Delta G(\sigma_i)/\Delta G(T)$ are shown in Figure 5(b). It is found that the peak value
51
52 is increased with an increase of b . However, it was also found that the peak value of the
53
54
55
56
57
58
59
60

specific value occurs almost at the same temperature, which is in a temperature range from 351.5 to 352.5K.

The frozen section and the activated section are then combined in parallel, and the storage modulus of the SMP was rewritten by using the frozen fraction. The storage modulus of SMPs has the following form at the transition temperature [12],

$$E(T) = \frac{1}{\frac{\phi_f}{E_i} + \frac{1-\phi_f}{E_e}} = \frac{E_i E_e}{\phi_f E_e + (1-\phi_f) E_i} \quad (13)$$

where E_i is the modulus of the SMP corresponding to the internal energetic deformation and is a constant within the studied temperature range. Symbol E_e is the modulus of the SMP corresponding to the entropic deformation. On the origin of the theory of rubber elasticity, the stress in the viscoelastic polymers is a nonlinear function with the extension strain [28]. Here, we used the experiment data reported in the previous work [12], which were obtained in the condition that the strain was not exceeding 10%. In this case, the relationship of the stress and strain is linear, therefore, E_e has the following expression,

$$E_e = 3Nk_B T \quad (14)$$

where N is the cross-link density.

By substituting equations (12) and (14) into (13), we obtain a new version of equation of the storage modulus,

$$E(T) = \frac{3Nk_B E_i T}{3Nk_B T + AT \exp\left(-\frac{\Delta G(T_h) 10^{\frac{-C_1(T-T_h)}{C_2+T-T_h}}}{RT} + \frac{T_h - T}{b \cdot T_h - T}\right)} (E_i - 3Nk_B T) \quad (15)$$

According to Liu et al [12], where $N=9.86 \times 10^{-4} \text{ mol cm}^{-3}$ and $E_i=813\text{MPa}$, the simulated relationship between the storage modulus and temperature is plotted in Figure 6 with an

1
2
3
4 increase in temperature from 333K to 343K, where the parameter b is increased from 1.02,
5
6 1.07, 1.12 to 1.17. While $b=1.07$ is **the condition for obtaining** the experimental results [29].
7
8

9 It is found that both the driving force and the frozen volume **have significant influences** on
10
11 the storage modulus of SMPs. When the value of b is close to 1.07, a small change in b will
12
13 have a significant influence on the storage modulus. However, the curves still have the same
14
15 tendency with increasing the driving force, while the storage modulus decreases at the same
16
17 temperature. Furthermore, these numerical results could be illustrated in combination of the
18
19 equations (4) and (5). The internal stress is increased with an increase in the value of b ,
20
21 **resulting in the decrease of the “frozen volume”**. As is well known, the SMPs are defined to
22
23 **have two or more segments, namely hard and soft segments [8-14]**. The “frozen volume” is
24
25 **used to characterize the volume fraction of soft segment**. The storage modulus is increased
26
27 **with the volume fraction of soft segment decreased, whereas simultaneously the volume**
28
29 **fraction of hard segments is increased**. The hard segment contributes more to the higher
30
31 **storage modulus than the soft one**. Therefore the storage modulus and other
32
33 **thermomechanical properties of the SMPs are increased with the volume fraction of soft**
34
35 **segment decreased**.
36
37
38
39
40
41
42
43
44

45 **3. Influence of internal stress on SME in a constraint recovery process of SMP**

46
47

48 As discussed in section 2 above, when **the SMP is in a** free recovery process, the internal
49
50 stress has a significant influence on the activation energy. In this section, when the shape
51
52 recovery behavior of the SMPs is driven by an external loading, influence of the internal
53
54 stress on the stress-strain constitutive relation and constraint SME **was investigated in order**
55
56 **to understand** the working mechanism of their thermomechanical performance.
57
58
59
60

At room temperature, the hard region represents the high modulus of elasticity material and its strain is small and proportional to the stress. Therefore, the constitutive equation was mainly established for the soft segments of the SMP which is viscoelastic at the applied stress. According to the transient network theory [29,30], the mobility of the amorphous SMP is restricted by the huge amount of physically/chemically cross-linked bonds. When considering the situation of an axial tensile loading and small strain, the proportion of the activated links caused by the internal stress is not apparently changed and can be set as $\chi(\vec{l})$. Accordingly, the proportion of the steady links is $1-\chi(\vec{l})$ without the external loading, where \vec{l} represents the recovery.

From the theory of absolute reaction rates, physical crosslinks in glassy polymers need to undergo a transition from a stable state to the active one [31]. The probability of this transition follows the Eyring equation and the results are presented in Figure 7. The breakage of steady links needs a free energy of ΔG_1 , and that of the activated links needs a free energy of ΔG_2 ($\Delta G_2 < \Delta G_1$).

The processes of breakage of the steady links and activated links are characterized using the functions $\Lambda_1(t, \vec{l})$ and $\Lambda_2(t, \vec{l})$, which describe the numbers of the steady links and the activated links at a time t , respectively. The quantity of breakage $\tilde{\Gamma}_i(t, \vec{l})$ at the time interval $[t, t + dt]$ is written as follow,

$$\tilde{\Gamma}_i(t, \vec{l}) = -\frac{\alpha}{\partial t} \Lambda_i(t, \vec{l}) \quad (16)$$

where i represents the number of transition processes of steady links and activated links, and the steady links change into active links only when $i=1$ and $i=2$, respectively. Here $\beta(t, \vec{l})$ is introduced to express the total numbers of frozen links in the soft segments of SMP with

the loading vector \vec{l} at a time of t and it has the following form,

$$\beta(t, \vec{l}) = \Lambda_1(t, \vec{l}) + \Lambda_2(t, \vec{l}) \quad (17)$$

The initial total number of the links equals to $\beta(0, \vec{l})$, thus the initial quantity of steady link ($\Lambda_1(0, \vec{l})$) and activated link ($\Lambda_2(0, \vec{l})$) can be written as,

$$\begin{cases} \Lambda_1(0, \vec{l}) = \beta(0, \vec{l}) \cdot [1 - \chi(\vec{l})] \\ \Lambda_2(0, \vec{l}) = \beta(0, \vec{l}) \cdot \chi(\vec{l}) \end{cases} \quad (18)$$

The kinetics of breakage $\Gamma_i(t, \vec{l})$ is determined by,

$$\Gamma_i(t, \vec{l}) = \frac{\tilde{\Gamma}_i(t, \vec{l})}{\Lambda_i(t, \vec{l})} \quad (19)$$

By integrating equations (16) and (19) with the initial condition equation (18), the quantity of steady link ($\Lambda_1(t, \vec{l})$) and activated link ($\Lambda_2(t, \vec{l})$) at a time t could be written as follows,

$$\begin{cases} \Lambda_1(t, \vec{l}) = \beta(0, \vec{l}) [1 - \chi(\vec{l})] \exp[-\int_0^t \Gamma_1(s, \vec{l}) ds] \\ \Lambda_2(t, \vec{l}) = \beta(0, \vec{l}) \chi(\vec{l}) \exp[-\int_0^t \Gamma_2(s, \vec{l}) ds] \end{cases} \quad (20)$$

Integrating equation (20) into (17), the total numbers of links ($\beta(t, \vec{l})$) exist in the time t are,

$$\beta(t, \vec{l}) = \beta(0, \vec{l}) \{ [1 - \chi(\vec{l})] \exp[-\int_0^t \Gamma_1(s, \vec{l}) ds] + \chi(\vec{l}) \exp[-\int_0^t \Gamma_2(s, \vec{l}) ds] \} \quad (21)$$

The function $w_i(t, \vec{l})$ is used to express the average potential energy of the steady links and activated links in the soft segment of SMP along the loading vector \vec{l} at the time t . The mechanical energy $W(t)$ is described by,

$$W(t) = \alpha \int_S \beta(t, \vec{l}) \cdot w(t, \vec{l}) \cdot dA(\vec{l}) \quad (22)$$

where S denotes the boundary of a unit sphere in the space of the loading vector \vec{l} , and the constant a is the density of the links and $dA(\vec{l})$ is the area element on S .

Cartesian coordinate frame $\{x_i\}$ was introduced here to set the position of the vector \vec{l} . Symbols of ϑ and φ were introduced to denote the spherical angles [Definitions are available as supplementary materials], the expanded form of equation (22) is as follows,

$$W(t) = a\beta(0, \vec{l}) \int_0^\pi \sin \vartheta d\vartheta \int_0^{2\pi} \left\{ \begin{aligned} & [1 - \chi(\vec{l})] \exp[-\int_0^t \Gamma_1(s, \vec{l})] w_1(t, \vec{l}) \\ & + \chi(\vec{l}) \exp[-\int_0^t \Gamma_2(s, \vec{l})] w_2(t, \vec{l}) \end{aligned} \right\} d\varphi \quad (23)$$

Now, if the kinetics of breakage $\Gamma_i(s, \vec{l})$ and the average potential energy $w_i(t, \vec{l})$ have been given, we can use equation (23) to describe the mechanical energy caused by the applied stress at the time t .

To analyze the average potential energy $w_i(t, \vec{l})$, the nominal strain $\varepsilon_*(t, \vec{l})$ in a nonlinear link has the following form [32],

$$\varepsilon_*(t, \vec{l}) = \vec{l} \cdot \hat{\varepsilon}(t) \cdot \vec{l} \quad (24)$$

where $\hat{\varepsilon}(t)$ is the infinitesimal (macro) strain tensor for transition from the initial configuration **into** its actual configuration at the current time t .

Both the steady link and the activated link are determined by assuming a nonlinear elastic spring with the mechanical energy,

$$w_1(t, \vec{l}) = \tilde{w}(\varepsilon_*) \quad (25)$$

At the condition of small strains, the calculation of potential energy of a link obeys the power-law stress-strain relation,

$$\tilde{w}(\varepsilon_*) = \frac{K}{1+k} |\varepsilon_*|^{1+k} \quad (26)$$

where both K and k are the constants [33].

However, the activated links initially have a quantity of potential energies that have the form of $(\Delta G_1 - \Delta G_2)$, thus,

$$w_2(t, \vec{l}) = w_1(t, \vec{l}) + \Delta G_1 - \Delta G_2 \quad (27)$$

Then, the theory of absolute reaction rate was used to analyze the kinetics of breakage of the steady links and the activated links. Meanwhile, considering the influence of applied stress, the probability for a steady link and an activated link to be broken within the time interval dt equals to,

$$\Gamma_i(t, \vec{l}) = m \exp\left(-\frac{\Delta G_i}{k_B \theta} + \frac{w_i(t, \vec{l})}{k_B \theta}\right) \quad (28)$$

where m is a constant, ΔG_i is the energy which breaks a steady link and an activated link, respectively. k_B denotes the Boltzmann's constant and θ is the absolute temperature. $\Gamma_i^0(t, \vec{l})$ is set as the invariant term to simplify equation (38) and **thus the following form can be obtained,**

$$\begin{cases} \Gamma_1^0(t, \vec{l}) = m \exp\left(-\frac{\Delta G_1}{k_B \theta}\right) \\ \Gamma_2^0(t, \vec{l}) = m \exp\left(-\frac{\Delta G_1 - 2\Delta G_2}{k_B \theta}\right) \end{cases} \quad (29)$$

Substituting equation (29) into (28), we can obtain,

$$\Gamma_i(t, \vec{l}) = \Gamma_i^0(t, \vec{l}) \exp\left(\frac{w_i(t, \vec{l})}{k_B \theta}\right) \quad (30)$$

By integrating equations (27) and (30) into (23), the mechanical energy $W(t)$ can be written as:

$$W(t) = a\beta(0, \vec{l}) \int_0^\pi \sin \vartheta d\vartheta \int_0^{2\pi} \left\{ \begin{aligned} & [1 - \chi(\vec{l})] \exp[-\Gamma_1^0(t, \vec{l})] \int_0^t \exp\left(\frac{w_1(s, \vec{l})}{k_B \theta}\right) ds w_1(t, \vec{l}) \\ & + \chi(\vec{l}) \exp[-\Gamma_2^0(t, \vec{l})] \int_0^t \exp\left(\frac{w_1(s, \vec{l})}{k_B \theta}\right) ds w_2(t, \vec{l}) \end{aligned} \right\} d\varphi \quad (31)$$

Differentiating equation (31) with respect to time t yields,

$$\begin{aligned}
\frac{dW(t)}{dt} &= a\beta(0, \vec{l}) \int_0^\pi \sin \vartheta d\vartheta \int_0^{2\pi} \left\{ \begin{aligned} & [1 - \chi(\vec{l})] \Gamma_1^0(t, \vec{l}) \exp[-\Gamma_1^0(t, \vec{l}) \int_0^t \exp(\frac{w_1(s, \vec{l})}{k_B \theta}) ds] \frac{w_1^2(t, \vec{l})}{k_B \theta} \\ & \chi(\vec{l}) \Gamma_1^0(t, \vec{l}) \exp[-\Gamma_2^0(t, \vec{l}) \int_0^t \exp(\frac{w_1(s, \vec{l})}{k_B \theta}) ds] \frac{w_1 \cdot w_2}{k_B \theta} \end{aligned} \right\} d\varphi \\
\frac{d \hat{\varepsilon}(t)}{dt} &- a\beta(0, \vec{l}) \int_0^\pi \sin \vartheta d\vartheta \int_0^{2\pi} \left\{ \begin{aligned} & [1 - \chi(\vec{l})] \Gamma_1^0(t, \vec{l}) \exp[-\Gamma_1^0(t, \vec{l}) \int_0^t \exp(\frac{w_1(s, \vec{l})}{k_B \theta}) ds] \frac{w_1^2(t, \vec{l})}{k_B \theta} \\ & + \chi(\vec{l}) \Gamma_1^0(t, \vec{l}) \exp[-\Gamma_2^0(t, \vec{l}) \int_0^t \exp(\frac{w_1(s, \vec{l})}{k_B \theta}) ds] \frac{w_1 \cdot w_2}{k_B \theta} \end{aligned} \right\} d\varphi
\end{aligned} \quad (32)$$

Now, a constitutive equation has been derived for an incompressible medium, and in this condition, the first invariant of the strain tensor $\hat{\varepsilon}$ disappears and the tensor $\hat{\varepsilon}$ coincides with the deviatoric part \hat{e} [33]. We can then obtain $\hat{\varepsilon}(t) = \hat{e}(t)$. By assuming the absolute temperature θ as a constant and neglecting the effect of thermal expansion, the form of differentiating of the mechanical energy can be written as [33],

$$\frac{dw}{dt} = \frac{1}{\rho} \hat{s} : \frac{d\hat{e}}{dt} - \frac{dQ}{dt} \quad (33)$$

where Q is the specific dissipation of energy, ρ is mass density and \hat{s} denotes the deviatoric part of the stress tensor.

By comparing equations (31) with (33), the final form of the deviatoric part of the stress tensor $\hat{s}(t)$ is described as,

$$\hat{s}(t) = a\beta(0, \vec{l}) \int_0^\pi \sin \vartheta d\vartheta \int_0^{2\pi} \left\{ \begin{aligned} & [1 - \chi(\vec{l})] \exp[-\Gamma_1^0(t, \vec{l}) \int_0^t \exp(\frac{w_1(s, \vec{l})}{k_B \theta}) ds] \frac{\partial w_1(t, \vec{l})}{\partial \hat{\varepsilon}(t)} \\ & + \chi(\vec{l}) \exp[-\Gamma_2^0(t, \vec{l}) \int_0^t \exp(\frac{w_1(s, \vec{l})}{k_B \theta}) ds] \frac{\partial w_2(t, \vec{l})}{\partial \hat{\varepsilon}(t)} \end{aligned} \right\} d\varphi \quad (34)$$

Because the ΔG_1 and ΔG_2 are independent of the loading time, the differentiation form of equations (26) and (27) can therefore be written as,

$$\frac{\partial w_1(t, \vec{l})}{\partial \varepsilon_0(t)} = \frac{\partial w_2(t, \vec{l})}{\partial \varepsilon_0(t)} = K \varepsilon_0(t)^k \left| \cos^2 \vartheta - \frac{1}{2} \sin^2 \vartheta \right|^{1+k} \quad (35)$$

When the loading strain rate is a constant and set by the symbol $\dot{\varepsilon}$, we can then obtain

$\varepsilon_0(t) = \dot{\varepsilon} \cdot t$. In equation (34), we simplify the term $\int_0^t \exp\left(\frac{w_1(s, \vec{l})}{k_B \theta}\right) ds$ at infinite small strains,

$$\begin{aligned} \int_0^t \exp\left(\frac{w_1(s, \vec{l})}{k_B \theta}\right) ds &= t + \int_0^t \frac{w_1(s, \vec{l})}{k_B \theta} ds \\ &= t + \frac{K}{(1+k)(2+k)k_B \theta} \dot{\varepsilon}^{1+k} t^{2+k} \left| \cos^2 \vartheta - \frac{1}{2} \sin^2 \vartheta \right|^{1+k} \end{aligned} \quad (36)$$

While the constant $\Delta = \frac{K}{(1+k)(2+k)k_B \theta}$ is introduced here to simplify equation (36),

and thus,

$$\int_0^t \exp\left(\frac{w_1(s, \vec{l})}{k_B \theta}\right) ds = t + \Delta \dot{\varepsilon}^{1+k} t^{2+k} \left| \cos^2 \vartheta - \frac{1}{2} \sin^2 \vartheta \right|^{1+k} \quad (37)$$

By setting $z = \cos \vartheta$, the deviatoric part of the stress tensor $\hat{s}(t)$ has the final form,

$$\begin{aligned} \hat{s}(t) &= 4\pi a K \beta(0, \vec{l}) \dot{\varepsilon}^k \int_0^1 \sqrt{1-z^2} \left[\frac{3}{2} z^2 - \frac{1}{2} \right]^{1+k} \cdot \\ &\left\{ \begin{aligned} &[1 - \chi(\vec{l})] \exp[-\Gamma_1^0(t, \vec{l}) (t + \Delta \dot{\varepsilon}^{1+k} t^{2+k} \left| \frac{3}{2} z^2 - \frac{1}{2} \right|^{1+k})] \\ &+ \chi(\vec{l}) \exp[-\Gamma_2^0(t, \vec{l}) (t + \Delta \dot{\varepsilon}^{1+k} t^{2+k} \left| \frac{3}{2} z^2 - \frac{1}{2} \right|^{1+k})] \end{aligned} \right\} dz \end{aligned} \quad (38)$$

Under an axial loading, σ_a is introduced as the applied stress along the loading direction, σ_2 and σ_3 are the stresses which are perpendicular to the loading direction. It is assumed that σ_i (the internal stress) is a constant, while the soft segment experiences a small strain.

By considering the boundary condition, one can obtain,

$$\sigma_a = -\sigma_i + s; \quad \sigma_2 = \sigma_3 = -\sigma_i - \frac{1}{2}s = 0, \quad \text{thus} \quad \sigma_a = \frac{3}{2}s \quad (39)$$

By substituting equation (39) into (38), the applied stress versus the strain rate has the

following form,

$$\sigma_a = \lambda \varepsilon^k \int_0^1 \sqrt{1-z^2} \left| \frac{3}{2} z^2 - \frac{1}{2} \right|^{1+k} \cdot \left\{ \begin{array}{l} [1-\chi(\vec{l})] \exp[-\Gamma_1^0(t, \vec{l}) \left(\frac{\varepsilon}{\varepsilon} + \Delta \frac{\varepsilon^{2+k}}{\varepsilon} \left| \frac{3}{2} z^2 - \frac{1}{2} \right|^{1+k} \right)] \\ + \chi(\vec{l}) \exp[-\Gamma_2^0(t, \vec{l}) \left(\frac{\varepsilon}{\varepsilon} + \Delta \frac{\varepsilon^{2+k}}{\varepsilon} \left| \frac{3}{2} z^2 - \frac{1}{2} \right|^{1+k} \right)] \end{array} \right\} dz \quad (40)$$

Here a constant $\lambda = 6\pi\alpha K\beta(0, \vec{l})$ is introduced to simplify equation (40) [Definitions are available as supplementary materials supplementary materials]. The comparisons between the numerical results of constitutive equation (40) and the experiment results [34] of the polyurethane SMP ($T_g=318\text{K}$) subjected to various tensions at $10^0/s$, $10^{-2}/s$ and $10^{-3}/s$ at the room temperature are shown in Figure 8. The values of parameters were chosen as $k=1$, $b=6552.079$, $\Gamma_1^0(t, \vec{l})=0.00576$, $\Gamma_2^0(t, \vec{l})=0.00727$, $\chi(t)=7\%$, $\Delta=243.25$. The frozen fractions $\chi(\vec{l})=7\%$ and $\Gamma_2^0(t, \vec{l})=0.00727$ were obtained. The activation speed has been increased slightly because of the decrease of activation energy caused by the internal stress. This constitutive relation not only characterizes the effect of internal stress on the activated fraction, but also models the mechanical behavior of the high sensitivity to the strain rate at a temperature of T_g for the SMP. This model also well predicts the dynamic responses of the SMPs at different strain rates. The relaxation time and the stretching time are not in the same order of magnitude, and the viscoelastic responses are easier generated at a lower strain rate because it needs a longer time for the breaking of links.

Furthermore, Figure 9 plots the numerical simulation results for the applied stress versus strain at different strain rates. It is found that the stress increases with an increase of the strain rate at the same strain. These numerical simulation results revealed the relationship between the external stress and internal stress [23]. With an increase in the strain rate, the effective

1
2
3
4 stress applied on the components in the polymers is increased, where the internal stress is a
5
6 constant value. Moreover, the applied stress is increased with an increase in the combined
7
8 external stress and internal stress. This indicates that the strain rate parameter has a direct
9
10 effect on the effective stress in the polymer, but has an indirect effect on the applied stress
11
12 according to the movement and the segmental relaxations of the cooperative segments in
13
14
15
16
17 polymers.

18
19 To find out the influence of the proportion of the activated volume, we increased the
20
21 proportion of the activated volume and maintained the activation energy of the activated links
22
23 unchanged, and the results are shown in Figure 10. The values of the proportion of the
24
25 activated volume are $\chi(\vec{l})=0, 20\%, 40\%$ and 60%. With the increase of the proportion of the
26
27 activated volume, much less stresses are needed for reaching the same strain because it needs
28
29 less energy when the proportion of the activated volume is increased. The numerical result
30
31 agrees well with the thermomechanical behavior of the SMPs. As is known, with an increase
32
33 of activated volume, the thermomechanical properties of the amorphous SMPs undergo a
34
35 transition from the glassy state to the rubbery state. The modulus is decreased in the transition
36
37 process, resulting in decrease of the stress. It is noted that the internal stress has an obvious
38
39 influence on the stress-strain constitutive relation even if the SMP is at room temperature.

40 41 42 43 44 45 46 47 48 **4. Conclusion**

49
50 “Frozen volume” transition model provides a classical approach for modelling the SME
51
52 and thermomechanical behavior of amorphous SMP, while viscoelastic model is suitable for
53
54 both SMPs and other types of amorphous polymers. However, the “frozen volume” parameter
55
56 is a phenomenologically temperature-dependent one and there is no physical meaning behind
57
58
59
60

1
2
3
4 it, **resulting in the difficulties** to model the mechanical behavior of SMPs. In this study,
5
6 “frozen volume” **was** initially introduced and a constitutive relation has been modelled with
7
8 the internal stress parameter according to the transient network theory and two-site model.
9
10 Phenomenological “frozen volume” transition is employed to explain the SME and shape
11
12 recovery behavior of SMPs, **and well predicts** the thermomechanical properties. Finally, the
13
14 simulation **results based on the proposed model were** compared with the experimental ones
15
16 reported in the literature. A good agreement between the theoretical and experimental results
17
18 has been shown. This phenomenological framework is expected to **provide a suitable** model
19
20 for amorphous SMPs on the origin of the phenomenological “frozen volume”.
21
22
23
24
25
26
27
28
29

30 **Acknowledgments**

31
32 The authors acknowledged the financial support from the National Natural Science
33
34 Foundation of China (NSFC) (Grant No. 11672642 and 11725208), UK Newton Mobility
35
36 Grant (IE161019) through Royal Society and the NSFC, and Royal academy of Engineering
37
38 UK-Research Exchange with China and India.
39
40
41
42
43
44

45 Data supporting the results and conclusions in the manuscript are available as supplementary
46
47 materials.
48
49
50
51
52
53
54
55
56
57
58
59
60

References

- [1] Wang Z L and Kang Z C 1998 Functional and smart materials *New York: Plenum Publishing corp.* pp: 514
- [2] Xie T 2011 Recent advances in shape memory polymer *Polymer* **52** 4985-5000
- [3] Huang W M, Yang B, An L, Li C and Chan Y S 2005 Water-driven programmable polyurethane shape memory polymer: demonstration and mechanism *Appl. Phys. Lett.* **86** 114105
- [4] Leng J S, Lv H B, Liu Y J and Du S Y 2007 Electroactivate shape-memory polymer filled with nanocarbon particles and short carbon fibers *Appl. Phys. Lett.* **91** 144105
- [5] Meng Q and Hu J 2009 A review of shape memory polymer composites and blends *Composites: Part A* **40** 1661-72
- [6] Lan X, Wang X H, Liu Y J, Leng J S and Du S Y 2009 Fiber reinforced shape-memory polymer composite and its application in a deployable hinge *Smart Mater. Struct.* **18** 024002
- [7] Davis K A and Burdick J A 2003 Photoinitiated crosslinked degradable copolymer network for tissue engineering applications *Biomaterials* **24** 2485-95
- [8] Chen Y C and Lagoudas D C 2008 A constitutive theory for shape memory polymers. Part I. large deformations *J. Mech. Phys. Solids* **56** 1752-65
- [9] Long K N, Dunn M L and Qi H J 2010 Mechanics of soft active materials with phase evolution *Int. J. Plast.* **26** 603-16
- [10] Chen X and Nguyen T D 2011 Influence of thermoviscoelastic properties and loading conditions on the recovery performance of shape memory polymers *Mech. Mater.* **43** 127-38
- [11] Yu K, Ge Q and Qi H J 2014 Reduced time as a unified parameter determining fixity and free recovery of shape memory polymers *Nat. Commun.* **5** 3066
- [12] Liu Y P, Gall K, Dunn M L, Greenberg A R and Diani J 2006 Thermomechanics of shape memory polymers: uniaxial experiments and constitutive modeling *Int. J. Plast.* **22** 279-313
- [13] Nguyen T D, Qi H J, Castro F and Long K N 2008 A thermoviscoelastic model for

- 1
2
3
4 amorphous shape memory polymers: incorporating structural and stress relaxation *J.*
5 *Mech. Phys. Solids.* **56** 2792-814
- 6
7 [14] Yu K, Xie T, Leng J S, Ding Y F and Qi H J 2012 Mechanisms of multi-shape memory
8 effects and associated energy release in shape memory polymers *Soft Matter* **8** 5687-95
- 9
10 [15] Yu K and Qi H J 2014 Temperature memory effect in amorphous shape memory
11 polymers *Soft Matter* **10** 9423-32
- 12
13 [16] Yu K, Ge Q and Qi H J 2014 Effects of stretch induced softening to the free recovery
14 behaviour of shape memory polymer composites *Polymer* **55** 5938-47
- 15
16 [17] White J R 1981 On internal stress and activation volume in polymers *J. Mater. Sci.* **16**
17 3249-62
- 18
19 [18] Diani J, Gilormini P, Frédy C and Rousseau I 2012 Predicting thermal shape memory of
20 crosslinked polymer networks from linear viscoelasticity *Int. J. Solids Struct.* **49** 793-9
- 21
22 [19] Ge Q, Yu K, Ding Y and Qi H J 2012 Prediction of temperature-dependent free recovery
23 behaviours of amorphous shape memory polymers *Soft Matter* **8** 11098-105
- 24
25 [20] Chen X and Nguyen T D 2011 Influence of thermoviscoelastic properties and loading
26 conditions on the recovery performance of shape memory polymers *Mech. Mater.* **43**
27 127-38
- 28
29 [21] Xiao R, Choi J, Lakhera N, Yakacki C M, Frick C P and Nguyen T D 2013 Modeling the
30 glass transition of amorphous networks for shape-memory behavior *J. Mech. Phys.Solids.*
31 **61** 1613-35.
- 32
33 [22] Guo X, Liu L, Liu Y, Zhou B and Leng J S 2014 Constitutive model for a stress- and
34 thermal-induced phase transition in a shape memory polymer *Smart. Mater. Struct.* **23**
35 105019
- 36
37 [23] Lu H B, Wang X D, Yu K, Huang W M, Yao Y T and Leng J S. 2017 A
38 Phenomenological formulation for the shape/temperature memory effect in amorphous
39 polymers with multi-stress components *Smart Mater. Struct.* **26** 095011
- 40
41 [24] Povolo F and Hermida E B 1995 Phenomenological description of strain rate and
42 temperature-dependent yield stress of PMMA *J. Appl. Polym. Sci.* **58** 55-68
- 43
44 [25] Povolo F, Schwartz G and Hermida E B 1996 Temperature and strain rate dependence of
45 the tensile yield stress of PVC *J. Appl. Polym. Sci.* **61** 109-17
- 46
47
48
49
50
51
52
53
54
55
56
57
58
59
60

- 1
2
3
4 [26] Brooks N W J, Duckett R A and Ward I M 1995 Modeling of double yield points in
5 polyethylene: temperature and strain rate dependence *J. Rheol.* **39** 425-36
6
7 [27] Kubat J and selden R 1978 The stress dependence of activation volumes in creep and
8 stress relaxation *Mat. Sci. Eng.* **36** 65-9
9
10 [28] Ward I M and Hadley D W 1993 An Introduction to the Mechanical Properties of Solid
11 Polymers *John Wiley & Sons, LTD, New York*
12
13 [29] Wang S Q 1992 Transient network theory for shear-thickening fluids and physically
14 crosslinked networks *Macromolecules* **25** 7003-10
15
16 [30] Tanaka F and Edwards S F 1992 Viscoelastic properties of physically crosslinked
17 networks. 1. Transient network theory *Macromolecules* **25** 183-90
18
19 [31] H. Eyring 1936 Viscosity, plasticity, and diffusion as examples of absolute reaction rates
20 *J. Chem. Phys.* **4** 283-91
21
22 [32] Drozdov, A. D. 1997 Modelling an anomalous stress relaxation in glassy polymers (the
23 kitagawa effect) *Math. Comput. Model.* **27** 45-67
24
25 [33] Drozdov, A. D. 1997 A model of adapative links in nonlinear viscoelasticity *J. Rheol.*
26 **41** 12223-45
27
28 [34] Pieczyska E A, Staszczak M, Maj M, Kowalczyk-Gajewska K, Golasinski K, Cristea M,
29 Tobushi H and Hayashi S 2016 Investigation of thermomechanical couplings, strain
30 localization and shape memory properties in a shape memory polymer subjected to
31 loading at various strain rates. *Smart Mater. Struct.* **25** 085002
32
33
34
35
36
37
38
39
40
41
42
43
44
45
46
47
48
49
50
51
52
53
54
55
56
57
58
59
60

Figure caption

Figure 1. Potential barrier for a molecule in the soft segments, showing the reduced energy produced by the driving force.

Figure 2. Comparisons between the fitting curve with the experimental results [12].

Figure 3. (a) The decrease of the activation energy caused by the driving force and the temperature. (b) The activation energy at the temperature range from 343 to 350K.

Figure 4. The influence of the parameter b on $\Delta G(\sigma_i)$: (a) $b=1.05, 1.07, 1.09, 1.11$ and 1.13 ; (b) $b=2, 3, 4, 5$ and 6 .

Figure 5. (a) The specific value between the decrease energy caused by the driving force and temperature. The peak value is 0.493 at temperature 351.5K . Below temperature 333K , the influence of the driving force is negligible. (b) The parameter $b=1.03, 1.04, 1.05$ and 1.06 : the peak value increases with the increase of parameter b and happens in almost same temperature.

Figure 6. The simulated curve of the elastic modulus: $b=1.02, 1.07, 1.12$ and 1.17 , respectively. $b=1.07$ is experimental value.

Figure 7. The energy needed to activate for the steady and activated links, respectively. The steady links need a free energy of ΔG_1 to be broken and the activated links need a free energy of ΔG_2 ($\Delta G_2 < \Delta G_1$) to be broken.

Figure 8. The simulation curve contrast with the experiment data [34] of the polyurethane SMP ($T_g=318\text{K}$) subjected to tension at $10^0/s, 10^{-2}/s$ and $10^{-3}/s$. The dot implicates the experiment data.

1
2
3
4 **Figure 9.** Numerical simulation for the relation between the stress of the SMP as a function
5
6 of extension ratio under a constant strain rate of $10^{-2}/s$, $10^{-2.5}/s$, $10^{-3}/s$ and $10^{-3.5}/s$,
7
8 respectively.
9

10
11 **Figure 10.** The simulation of the activated volume with $\chi(\vec{l})=0\%$, 20%, 40% and 60%.
12
13
14
15
16
17
18
19
20
21
22
23
24
25
26
27
28
29
30
31
32
33
34
35
36
37
38
39
40
41
42
43
44
45
46
47
48
49
50
51
52
53
54
55
56
57
58
59
60

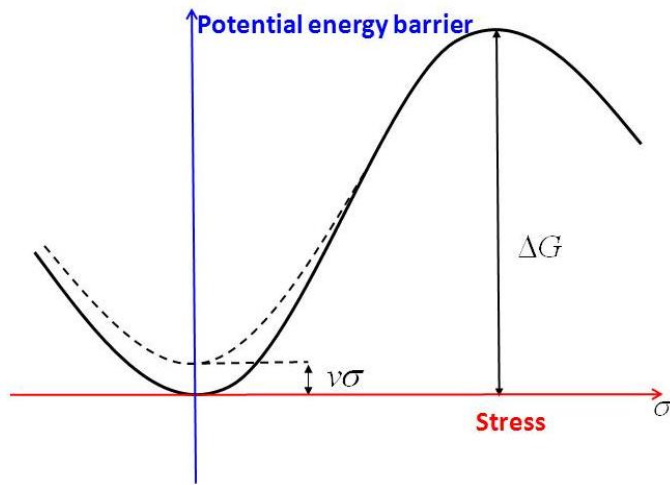


Figure 1. Potential barrier for a molecule in the soft segments, showing the reduced energy produced by the driving force.

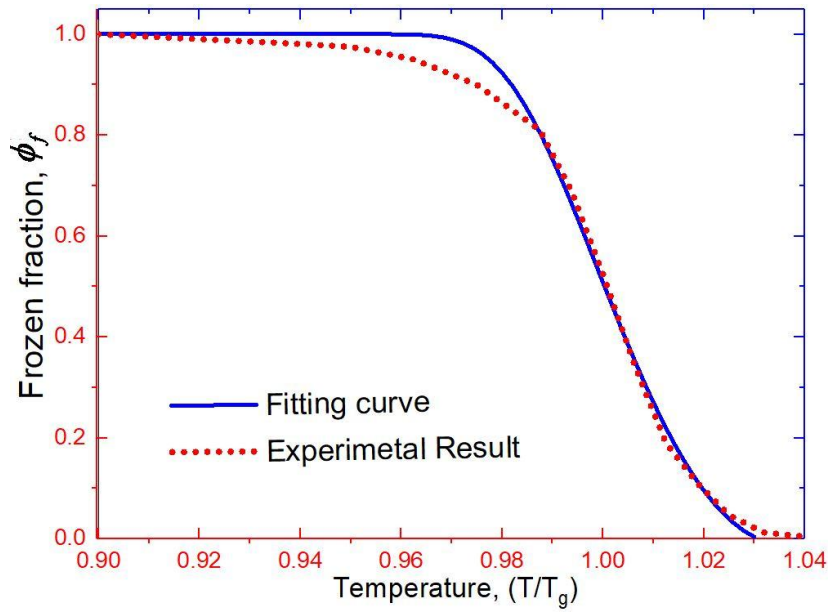


Figure 2. Comparisons between the fitting curve with the experimental results [12].

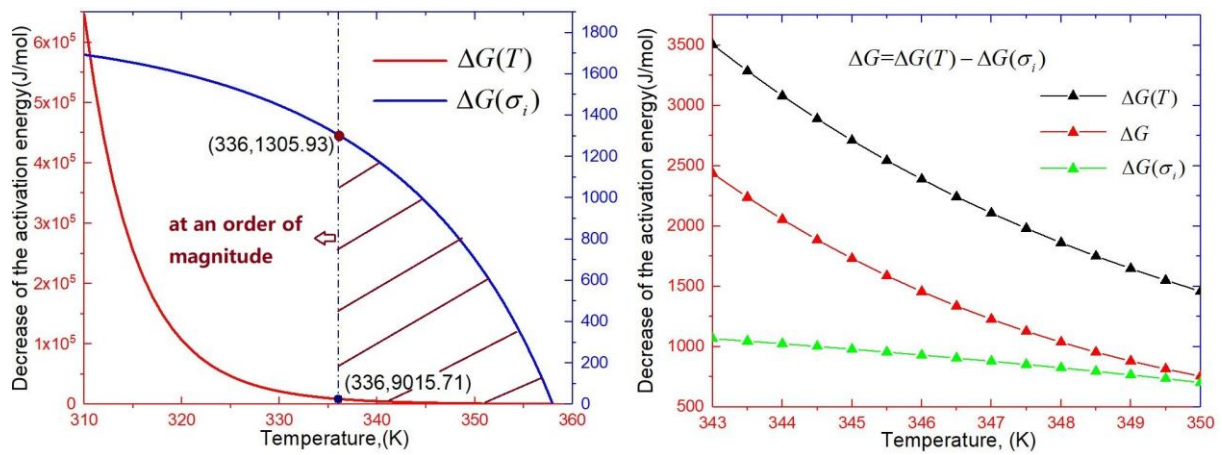


Figure 3. (a) The decrease of the activation energy caused by the driving force and the temperature. (b) The activation energy at the temperature range from 343 to 350K.

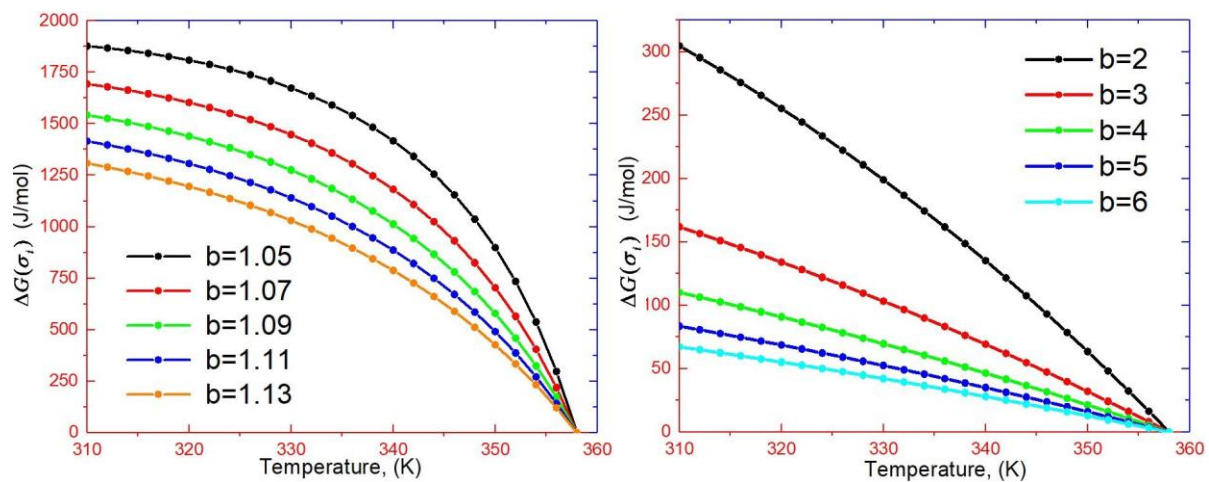


Figure 4. The influence of the parameter b on $\Delta G(\sigma_i)$: (a) $b=1.05, 1.07, 1.09, 1.11$ and 1.13 ;
(b) $b=2, 3, 4, 5$ and 6 .

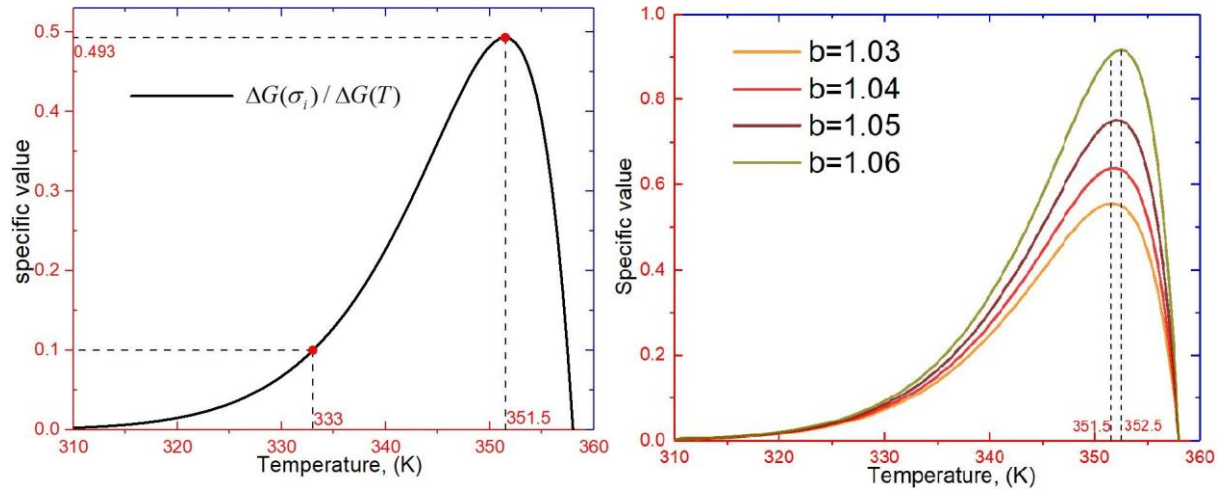


Figure 5. (a) The specific value between the decrease energy caused by the driving force and temperature. The peak value is 0.493 at temperature 351.5K. Below temperature 333K, the influence of the driving force is negligible. (b) The parameter $b=1.03, 1.04, 1.05$ and 1.06 : the peak value increases with the increase of parameter b and happens in almost same temperature.

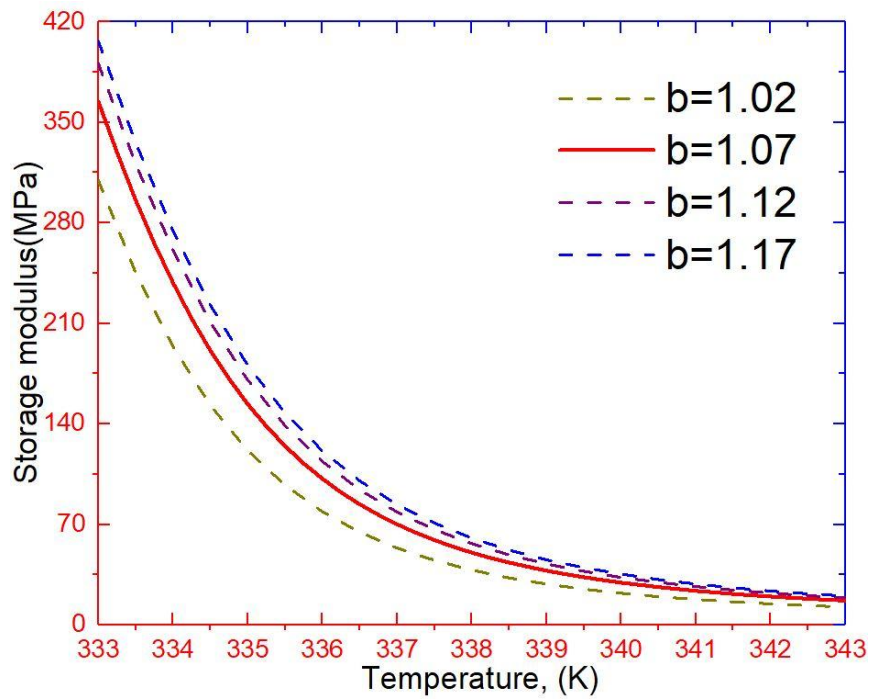


Figure 6. The simulated curve of the elastic modulus: $b=1.02$, 1.07 , 1.12 and 1.17 , respectively. $b=1.07$ is experimental value.

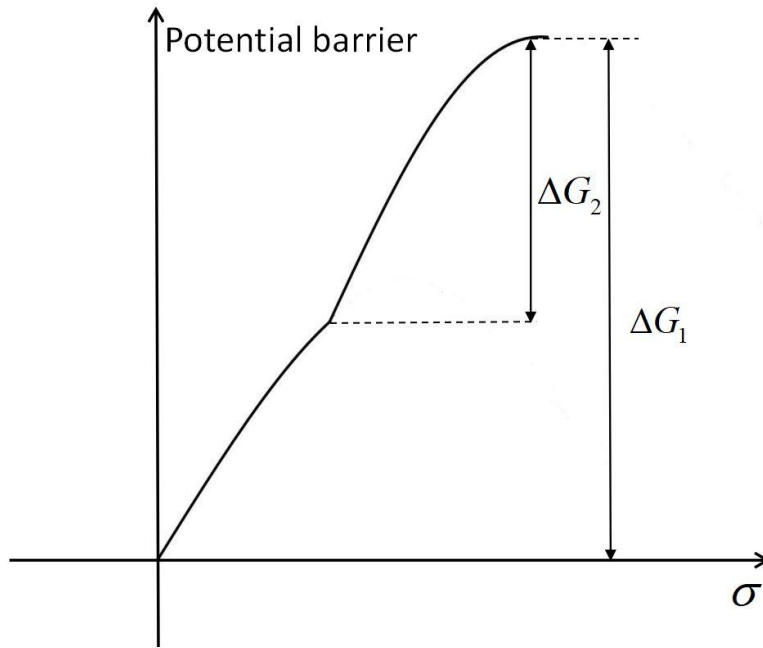


Figure 7. The energy needed to activate for the steady and activated links, respectively. The steady links need a free energy of ΔG_1 to be broken and the activated links need a free energy of ΔG_2 ($\Delta G_2 < \Delta G_1$) to be broken.

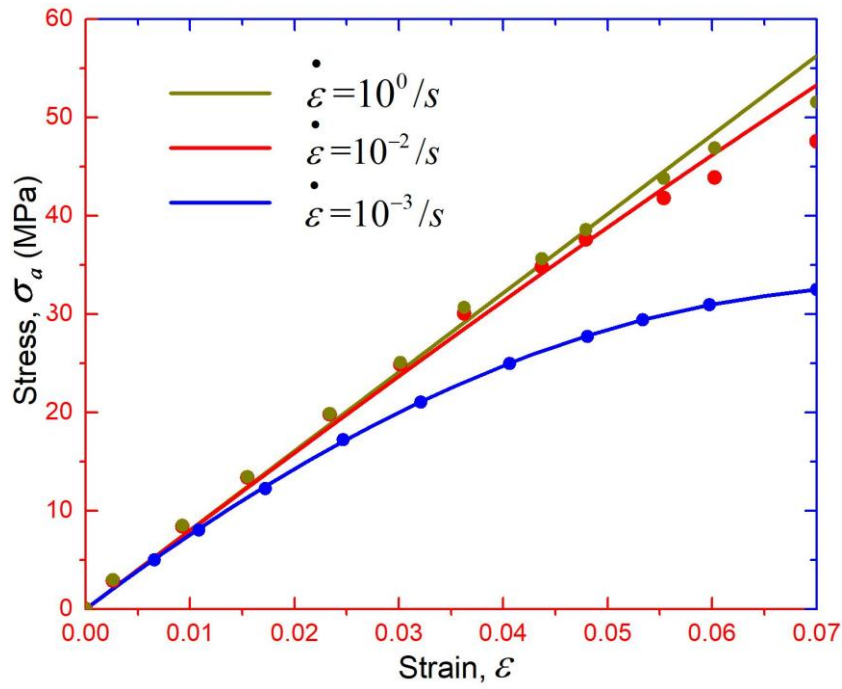


Figure 8. The simulation curve contrast with the experiment data [34] of the polyurethane SMP ($T_g=318\text{K}$) subjected to tension at $10^0/s$, $10^{-2}/s$ and $10^{-3}/s$. The dot implicates the experiment data.

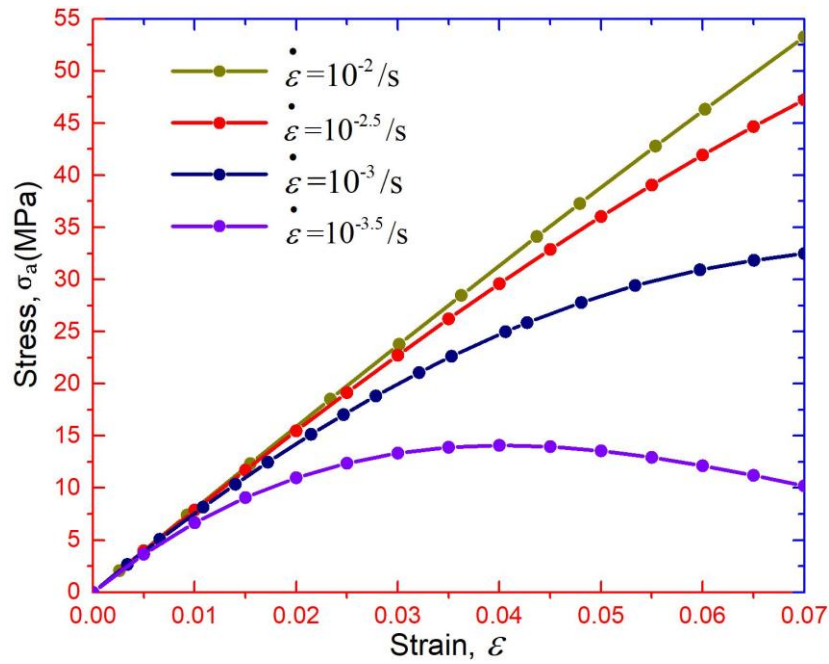


Figure 9. Numerical simulation for the relation between the stress of the SMP as a function of extension ratio under a constant strain rate of $10^{-2}/s$, $10^{-2.5}/s$, $10^{-3}/s$ and $10^{-3.5}/s$, respectively.

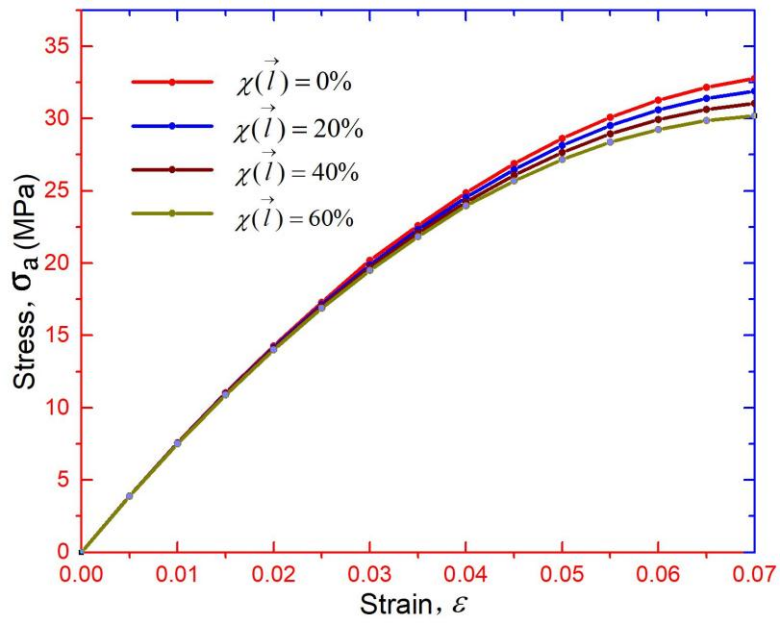


Figure 10. The simulation of the activated volume with $\chi(\vec{l})=0\%$, 20%, 40% and 60%.